Opto-Electronic Advances

Supplementary information

2022, Vol. 5, No. 3

DOI: 10.29026/oea.2022.210052

Ultrashort pulsed laser induced complex surface structures generated by tailoring the melt hydrodynamics

Fotis Fraggelakis[1]*, George D. Tsibidis[1,2]* and Emmanuel Stratakis[1,2]*

[1]Institute of Electronic Structure and Laser (IESL), Foundation for Research and Technology (FORTH), N. Plastira 100, Vassilika Vouton, Heraklion 70013, Greece; [2]Department of Physics, University of Crete, Heraklion 71003, Greece.

*Correspondence: F Fraggelakis, E-mail: fraggelakis@iesl.forth.gr; GD Tsibidis, E-mail: tsibidis@iesl.forth.gr;
E Stratakis, E-mail: stratak@iesl.forth.gr

This file includes:

Supplementary information for this paper is available at https://doi.org/10.29026/oea.2022.210052

Section 1: Temperature profiles and fluid movement

Simulations results and enlarged images that illustrate the temperature profiles and molten material transport at the timepoints t = 490 ps (before the second of the double pulse train irradiates the material) and t = 520 ps (after thermalisation following the impact of the second pulse) are presented below for NP = 50. Results are classified according to the order of the pulses in the sequence (see main text for further explanation). The size of the velocity vectors that indicate the fluid movement are rescaled to the maximum lattice temperature value attained at each time point. The direction of the vectors indicate the fluid direction based on the temperature gradient (i.e. spatial change of the temperature). *White* dots that appear is some regions indicate a stagnant behaviour (i.e. nearly immobile fluid). A *blue-to-red* colorbar was used to emphasise better the range of temperature values and indicate more clearly the fluid direction.

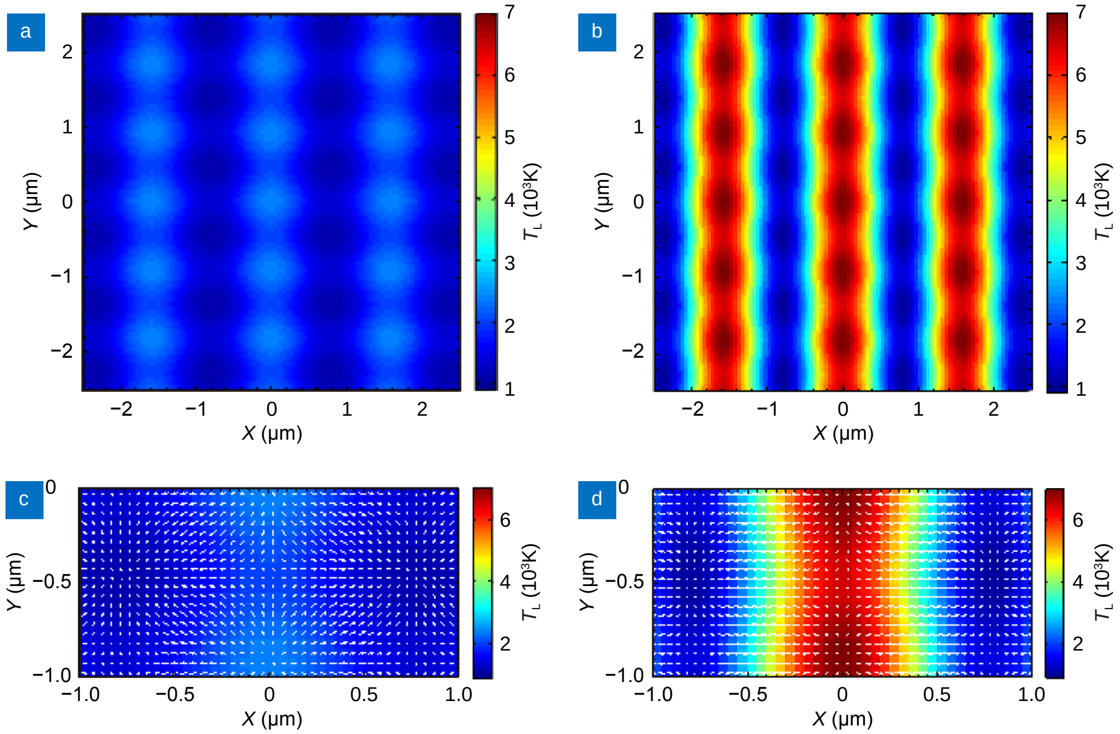

Fig. S1 | *G* + *V*: Temperature profiles at (**a**) t = 490 ps and (**b**) t = 520 ps. Fluid movement is illustrated in (**c**) and (**d**) for t = 490 ps and t = 520 ps, respectively.

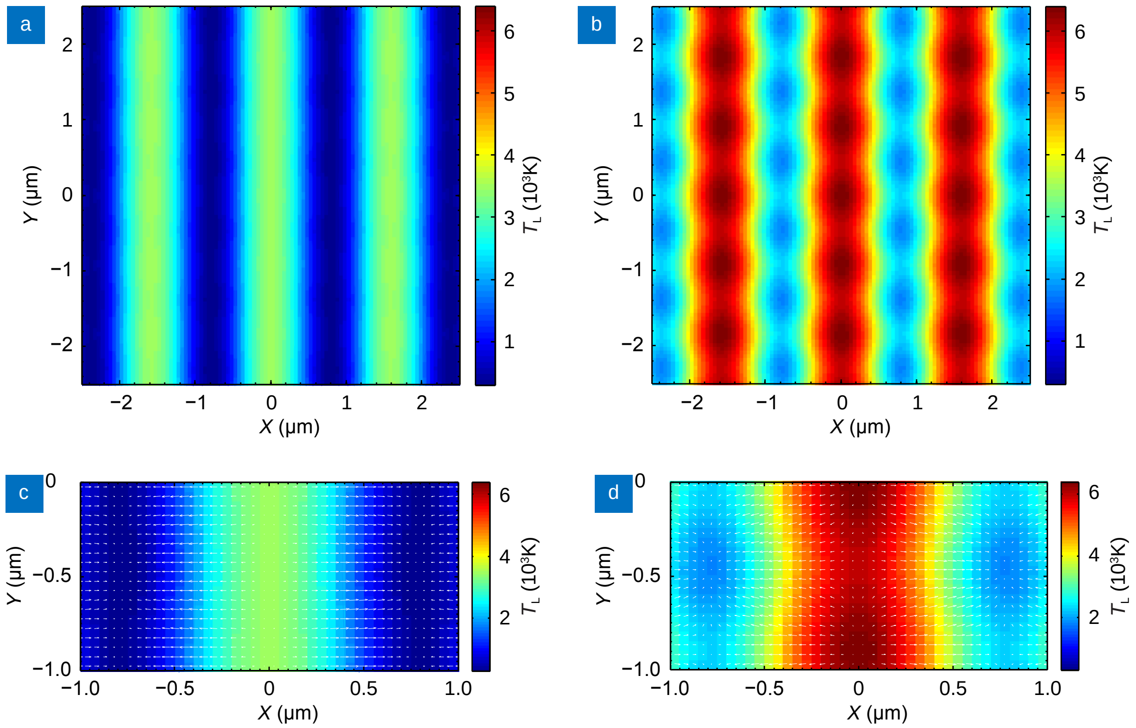

Fig. S2 | *V* + *G*: Temperature profiles at (**a**) *t* = 490 ps and (**b**) *t* = 520 ps. Fluid movement is illustrated in (**c**) and (**d**) for *t* = 490 ps and *t* = 520 ps, respectively.

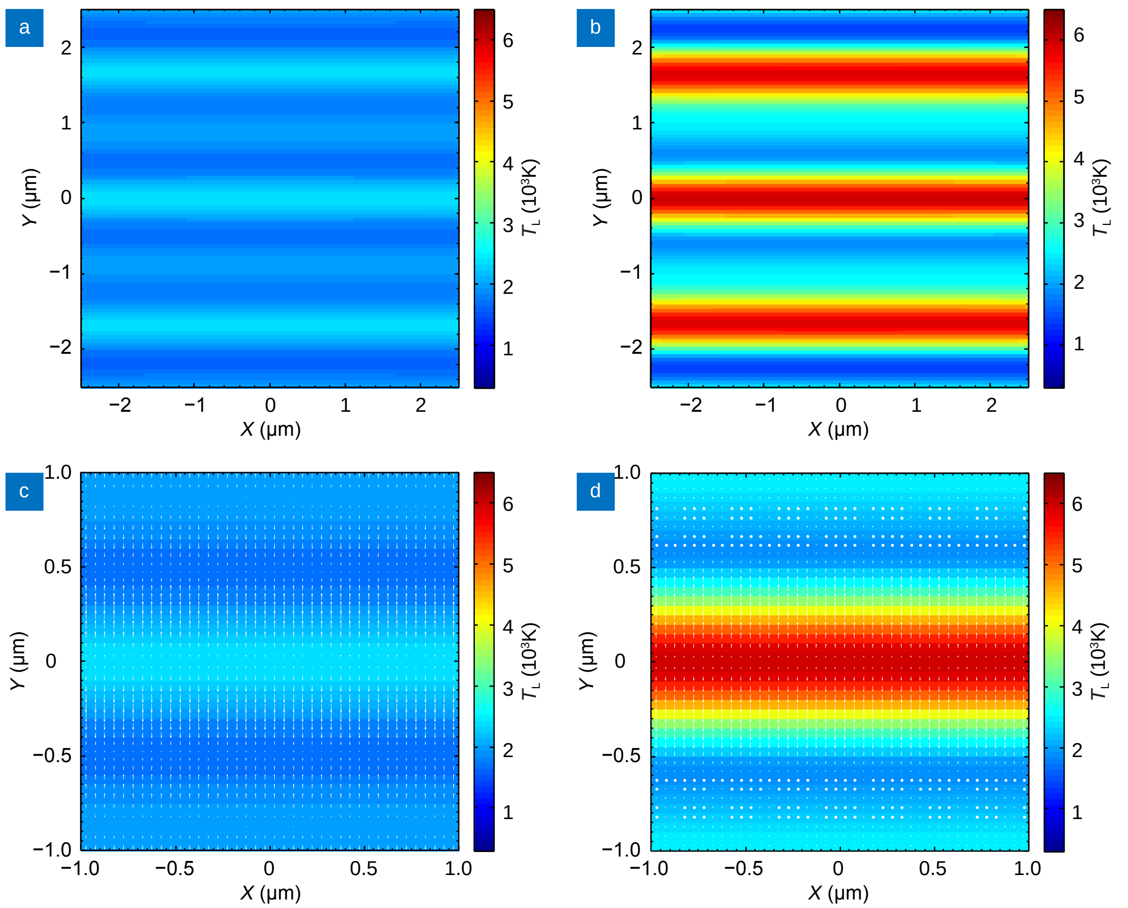

Fig. S3 | *G* + *H*: Temperature profiles at (**a**) *t* = 490 ps and (**b**) *t* = 520 ps. Fluid movement is illustrated in (**c**) and (**d**) for *t* = 490 ps and *t* = 520 ps, respectively.

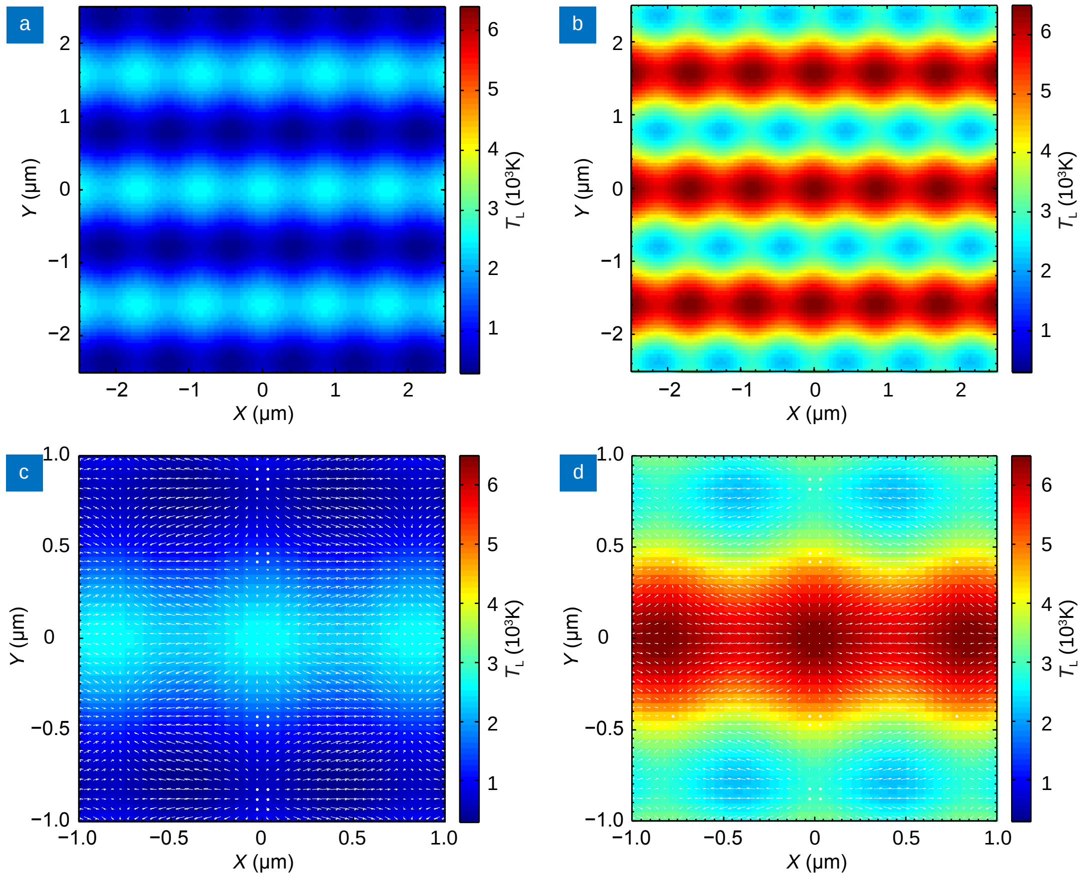

Fig. S4 | *H* + *G*: Temperature profiles at (**a**) *t* = 490 ps and (**b**) *t* = 520 ps. Fluid movement is illustrated in (**c**) and (**d**) for *t* = 490 ps and *t* = 520 ps, respectively.

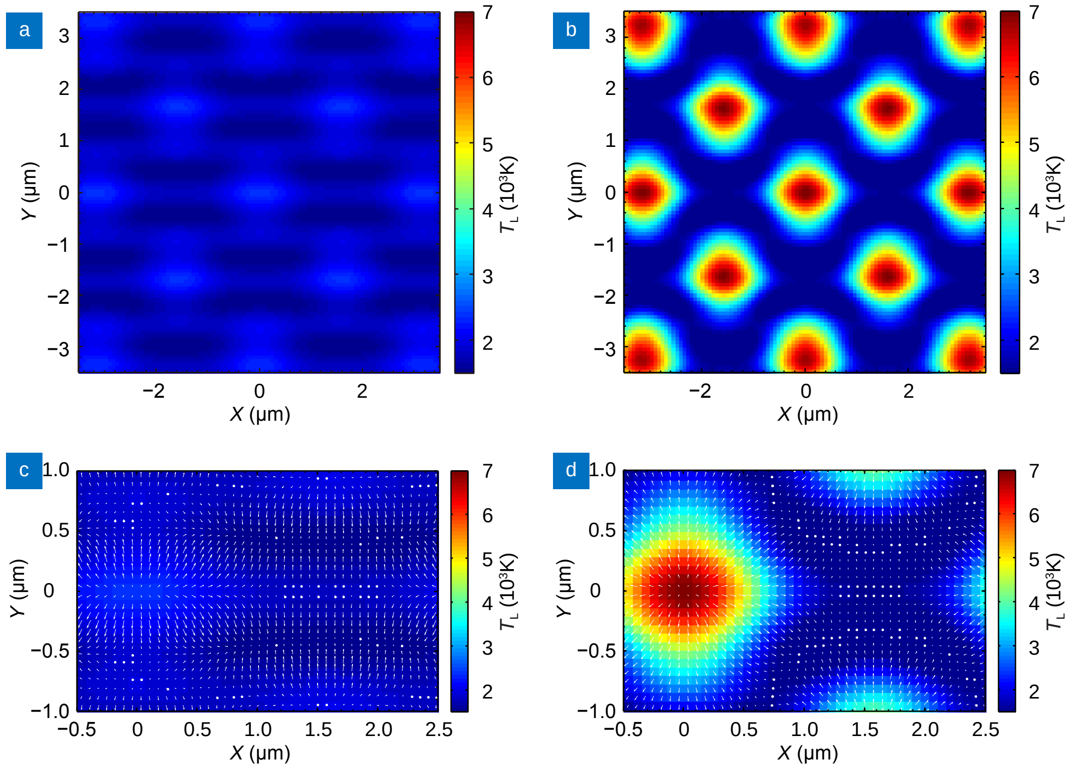

Fig. S5 | *G* + *D*: Temperature profiles at (**a**) *t* = 490 ps and (**b**) *t* = 520 ps. Fluid movement is illustrated in (**c**) and (**d**) for *t* = 490 ps and *t* = 520 ps, respectively.

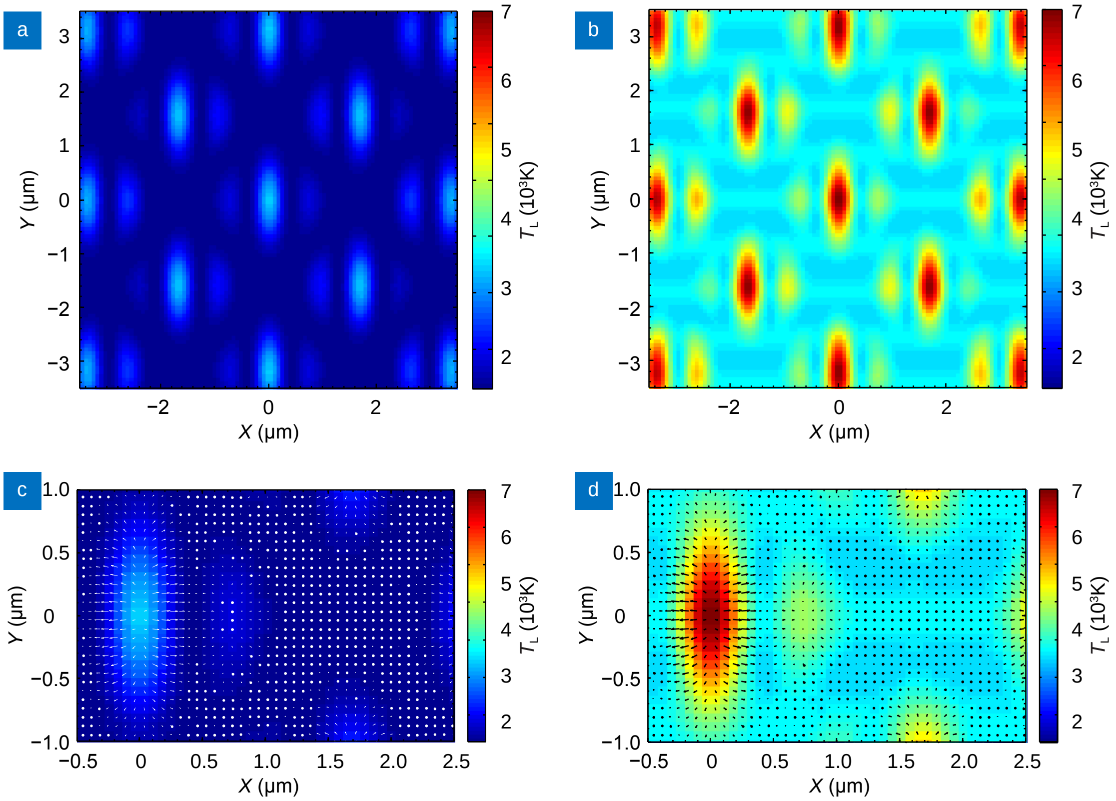

Fig. S6 | *D* + *G*: Temperature profiles at (**a**) *t* = 490 ps and (**b**) *t* = 520 ps. Fluid movement is illustrated in (**c**) and (**d**) for *t* = 490 ps and *t* = 520 ps, respectively.

Section 2: Temperature profiles and fluid movement for *NP* = 2 and *NP* = 5 (for *G* + *V*)

To illustrate the impact of the surface topography and describe quantitatively the interpulse surface pattern changes, temperature profiles are shown for *NP* = 2 (Fig. S7) and *NP* = 5 (Fig. S8) at *t* = 490 ps and *t* = 520 ps for *G* + *V*. *White* dots that appear is some regions indicate a stagnant behaviour (i.e. nearly immobile fluid). In (c) and (d) a *blue-to-red* colorbar was used to emphasise better the range of temperature values and indicate more clearly the fluid direction. By contrast, a *red-to-white* colorbar was used in (a) and (b) (similar to the one used in the main manuscript).

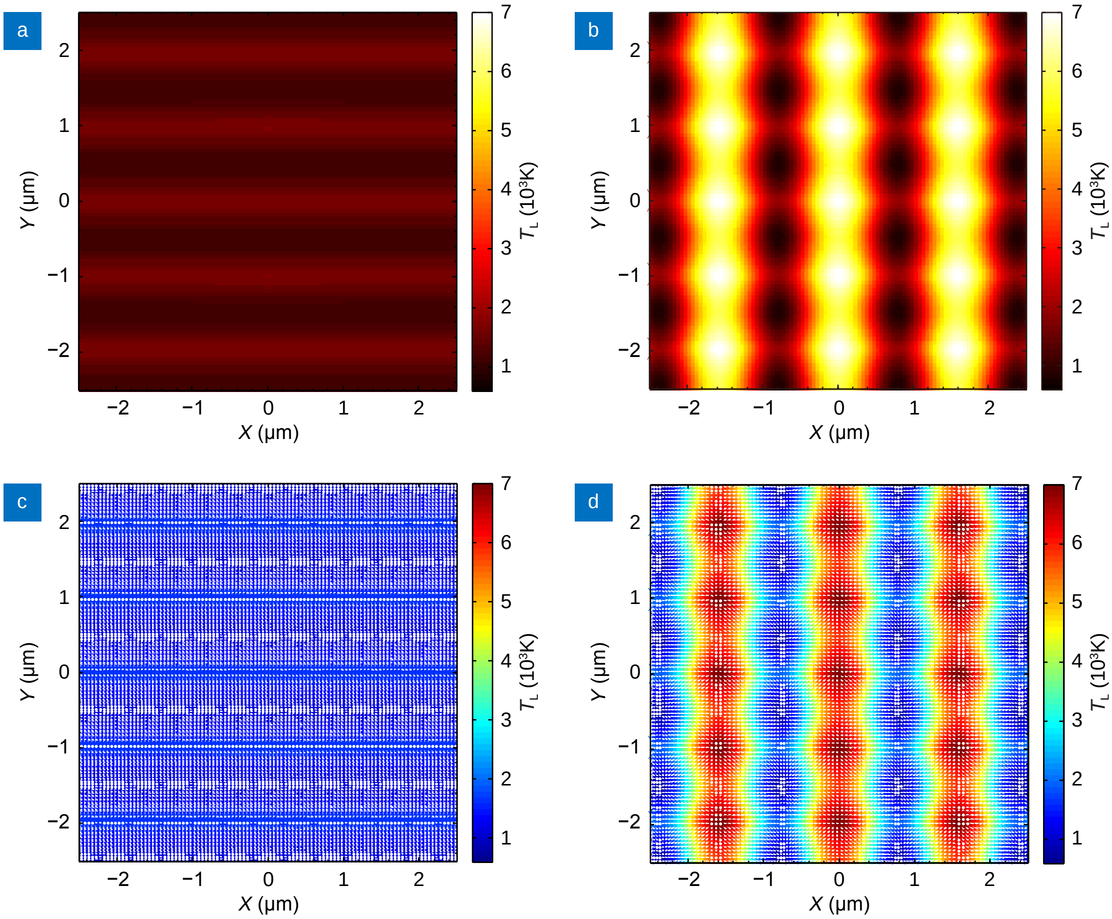

Fig. S7 | Temperature profiles for *G* + *V* at (**a**, **c**) *t* = 490 ps and (**b**, **d**) *t* = 520 ps for *NP* = 2. Fluid movement is illustrated in (c) and (d) for *t* = 490 ps and *t* = 520 ps, respectively.

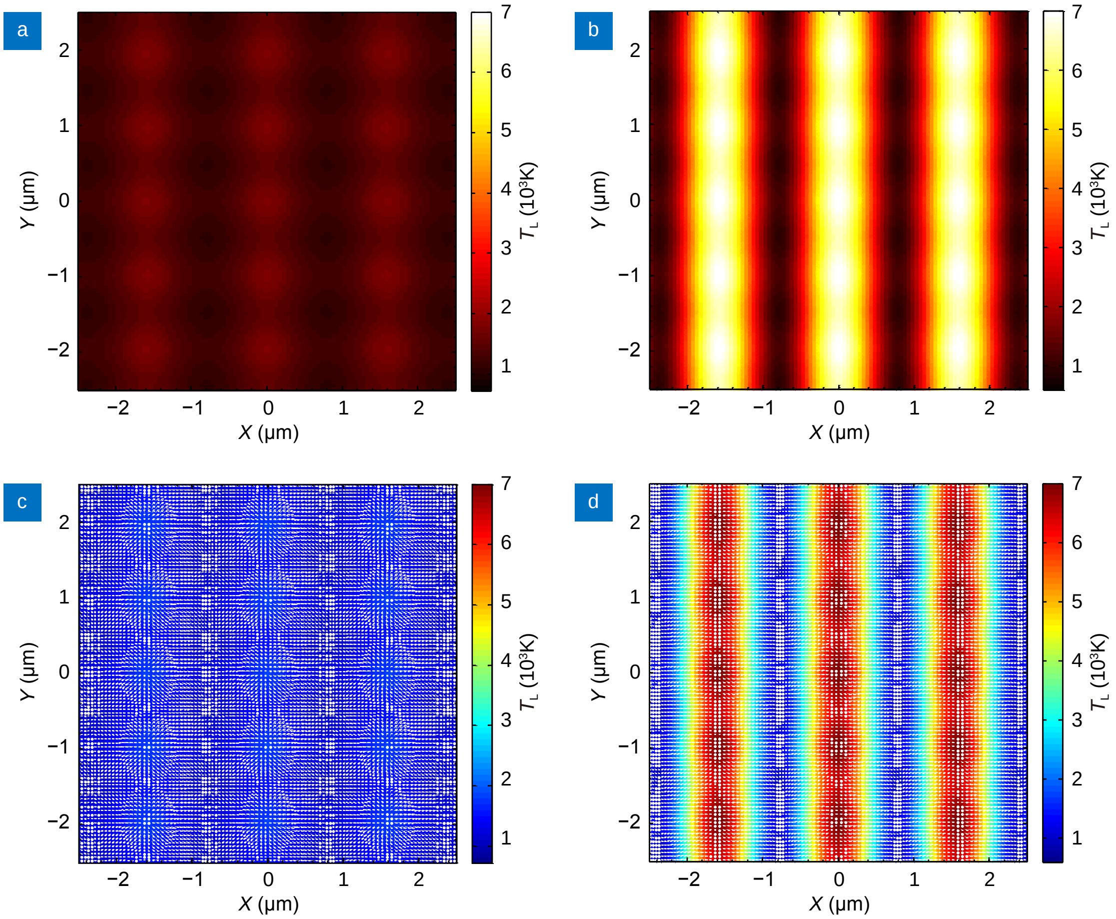

Fig. S8 | Temperature profile at (**a**, **c**) t = 490 ps and (**b**, **d**) t = 520 ps for NP = 5. Fluid movement is illustrated in (c) and (d) for t = 490 ps and t = 520 ps, respectively.

Section 3: Total intensity profile

The laser intensity of the Gaussian profile is given by

$$I_{\text{Gaussian}}= A\mathrm{e}^{-4\ln2\left(\frac{t-3\tau_{\text{p}}}{\tau_{\text{p}}}\right)^2}\mathrm{e}^{-2\left(\frac{x^2+y^2}{R_0^2}\right)}= P_1\mathrm{e}^{-4\ln2\left(\frac{t-3\tau_{\text{p}}}{\tau_{\text{p}}}\right)^2}\ , \tag{S1}$$

where $P_1 \equiv A\mathrm{e}^{-2\left(\frac{x^2+y^2}{R_0^2}\right)}$, and A contains the pulse duration and fluence[1].

By contrast, the DLIP intensity is provided by the expression

$$I_{\text{DLIP}}= BI_0^{(i)}\mathrm{e}^{-4\ln2\left(\frac{t-3\tau_{\text{p}}}{\tau_{\text{p}}}\right)^2}\mathrm{e}^{-2\left(\frac{x^2+y^2}{R_0^2}\right)}= P_2\mathrm{e}^{-4\ln2\left(\frac{t-3\tau_{\text{p}}}{\tau_{\text{p}}}\right)^2}\ , \tag{S2}$$

where $P_2 \equiv BI_0^{(i)}\mathrm{e}^{-2\left(\frac{x^2+y^2}{R_0^2}\right)}$ (i = 2 or 4 for a DLIP with two or four laser pulses, respectively, as given in Eq. (S1) in the main text) while B contains the pulse duration and fluence[2].

Assuming that there is a temporal separation between the two pulses (equal to $\Delta\tau$), there are two possibilities for the total intensity that depends on which pulse irradiates the material first

$$I_{\text{total}}\left(t,x,y,surface\right)=\left[P_1\mathrm{e}^{-4\ln2\left(\frac{t-3\tau_p}{\tau_p}\right)^2}+P_2\mathrm{e}^{-4\ln2\left(\frac{t-3\tau_p-\Delta\tau}{\tau_p}\right)^2}\right]\ , \tag{S3}$$

if the Gaussian pulse *precedes* the DLIP pulse

and

$$I_{\text{total}}\left(t,x,y,surface\right)=\left[P_2 e^{-4\ln2\left(\frac{t-3\tau_{\text{p}}}{\tau_{\text{p}}}\right)^2}+P_1 e^{-4\ln2\left(\frac{t-3\tau_{\text{p}}-\Delta\tau}{\tau_{\text{p}}}\right)^2}\right]\ , \tag{S4}$$

if the Gaussian pulse *follows* the DLIP pulse.

We can write Eqs. (S3), (S4) in a compact form in which $G_1=0, G_2=1$ (Eq. (S3)) and $G_1=1, G_2=0$ (Eq. (S4)).

$$I_{\text{total}}\left(t,x,y,surface\right)=\left[P_1\mathrm{e}^{-4\ln2\left(\frac{t-3\tau_{\text{p}}-G_1\Delta\tau}{\tau_{\text{p}}}\right)^2}+P_2\mathrm{e}^{-4\ln2\left(\frac{t-3\tau_{\text{p}}-G_2\Delta\tau}{\tau_{\text{p}}}\right)^2}\right]\ . \tag{S5}$$

Section 4: Navier-Stokes equations

Below, the Navier-Stokes equations (for an incompressible fluid $\vec{\nabla}\cdot\vec{\boldsymbol{u}}=0$) are presented in a matrix form in 3D[3]. We know that

$$\rho_0\left(\frac{\partial\vec{\boldsymbol{u}}}{\partial t}+\vec{\boldsymbol{u}}\cdot\vec{\nabla}\vec{\boldsymbol{u}}\right)=\vec{\nabla}\cdot\left(-P\mathbf{1}+\mu\left(\vec{\nabla}\vec{\boldsymbol{u}}\right)+\mu\left(\vec{\nabla}\vec{\boldsymbol{u}}\right)^T\right)\ , \tag{S6}$$

where

$$\left(\vec{\nabla}\vec{\boldsymbol{u}}\right)=\begin{pmatrix}\frac{\partial u}{\partial x} & \frac{\partial v}{\partial x} & \frac{\partial w}{\partial x}\\ \frac{\partial u}{\partial y} & \frac{\partial v}{\partial y} & \frac{\partial w}{\partial y}\\ \frac{\partial u}{\partial z} & \frac{\partial v}{\partial z} & \frac{\partial w}{\partial z}\end{pmatrix},\left(\vec{\nabla}\vec{\boldsymbol{u}}\right)^T=\begin{pmatrix}\frac{\partial u}{\partial x} & \frac{\partial u}{\partial y} & \frac{\partial u}{\partial z}\\ \frac{\partial v}{\partial x} & \frac{\partial v}{\partial y} & \frac{\partial v}{\partial z}\\ \frac{\partial w}{\partial x} & \frac{\partial w}{\partial y} & \frac{\partial w}{\partial z}\end{pmatrix}, P\mathbf{1}=\begin{pmatrix}P & 0 & 0\\ 0 & P & 0\\ 0 & 0 & P\end{pmatrix}, \text{and } \vec{\boldsymbol{u}}=(u,v,w)$$

After the calculations, we obtain the following formulae in matrix form (by taking into account that the fluid is incompressible)

$$\begin{aligned}\rho_0\left(\frac{\partial u}{\partial t}+u\frac{\partial u}{\partial x}+v\frac{\partial u}{\partial y}+w\frac{\partial u}{\partial z}\right)&=-\frac{\partial P}{\partial x}+\mu\left(\frac{\partial^2 u}{\partial x^2}+\frac{\partial^2 u}{\partial y^2}+\frac{\partial^2 u}{\partial z^2}\right)\\ \rho_0\left(\frac{\partial v}{\partial t}+u\frac{\partial v}{\partial x}+v\frac{\partial v}{\partial y}+w\frac{\partial v}{\partial z}\right)&=-\frac{\partial P}{\partial y}+\mu\left(\frac{\partial^2 v}{\partial x^2}+\frac{\partial^2 v}{\partial y^2}+\frac{\partial^2 v}{\partial z^2}\right)\\ \rho_0\left(\frac{\partial w}{\partial t}+u\frac{\partial w}{\partial x}+v\frac{\partial w}{\partial y}+w\frac{\partial w}{\partial z}\right)&=-\frac{\partial P}{\partial z}+\mu\left(\frac{\partial^2 w}{\partial x^2}+\frac{\partial^2 w}{\partial y^2}+\frac{\partial^2 w}{\partial z^2}\right)\ .\end{aligned} \tag{S7}$$

Equation (S7) represents the standard notation of NSE.

Section 5: Surface patterns

In the following figures, we illustrate enlarged contour plots of the surface patterns in which depth variation is shown (enlarged contour plots shown in last column of Fig. S4 in the main text).

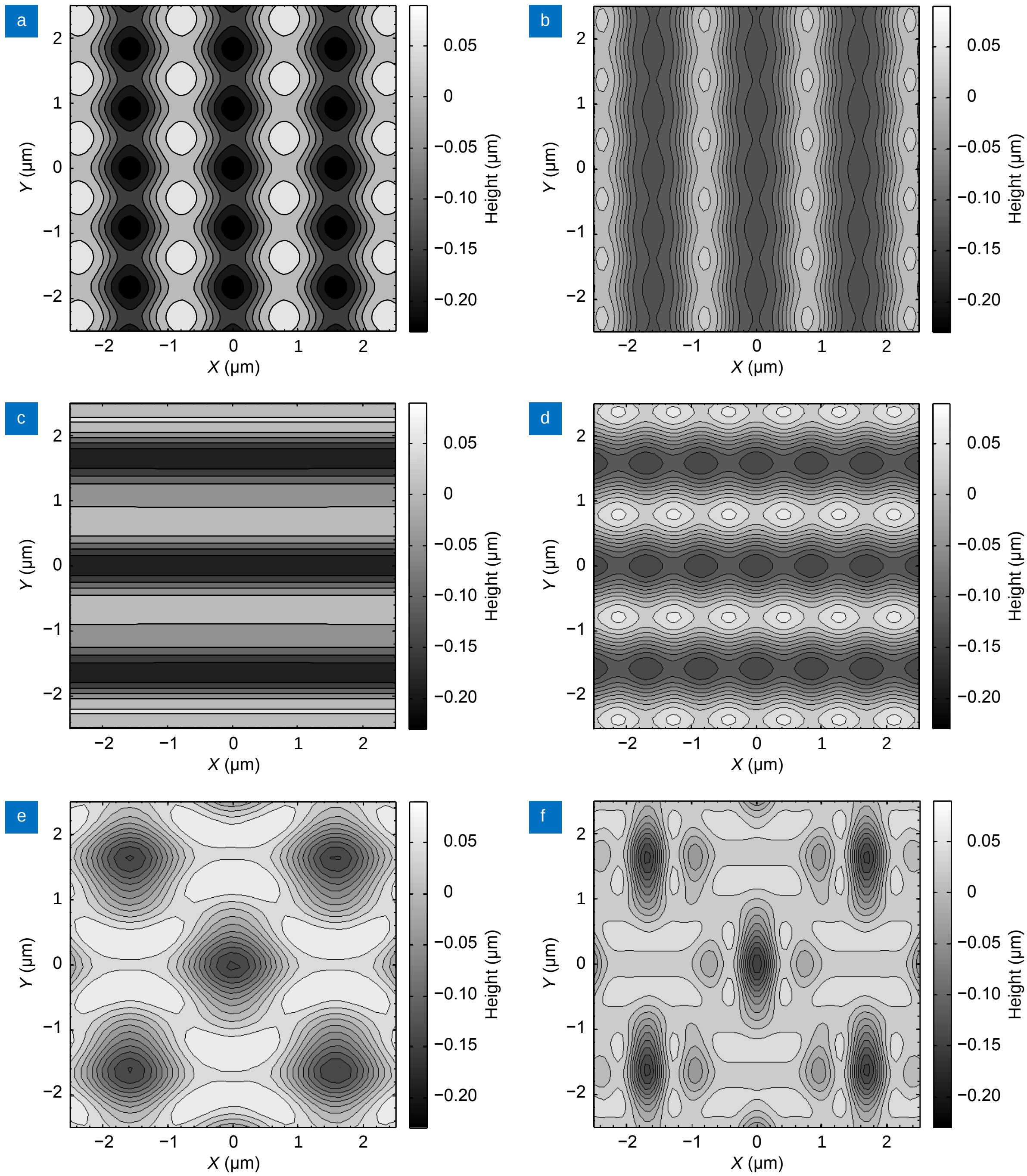

Fig. S9 | Surface contour plots for *NP* = 50 for (**a**) *G* + *V*, (**b**) *V* + *G*, (**c**) *G* + *H*, (**d**) *H* + *G*, (**e**) *G* + *D*, (**f**) *G* + *D*

Section 6: Surface distribution of height

In the following figures, we illustrate surface patterns in which surface distribution of height is shown (in a 'blue to red' colorbar)

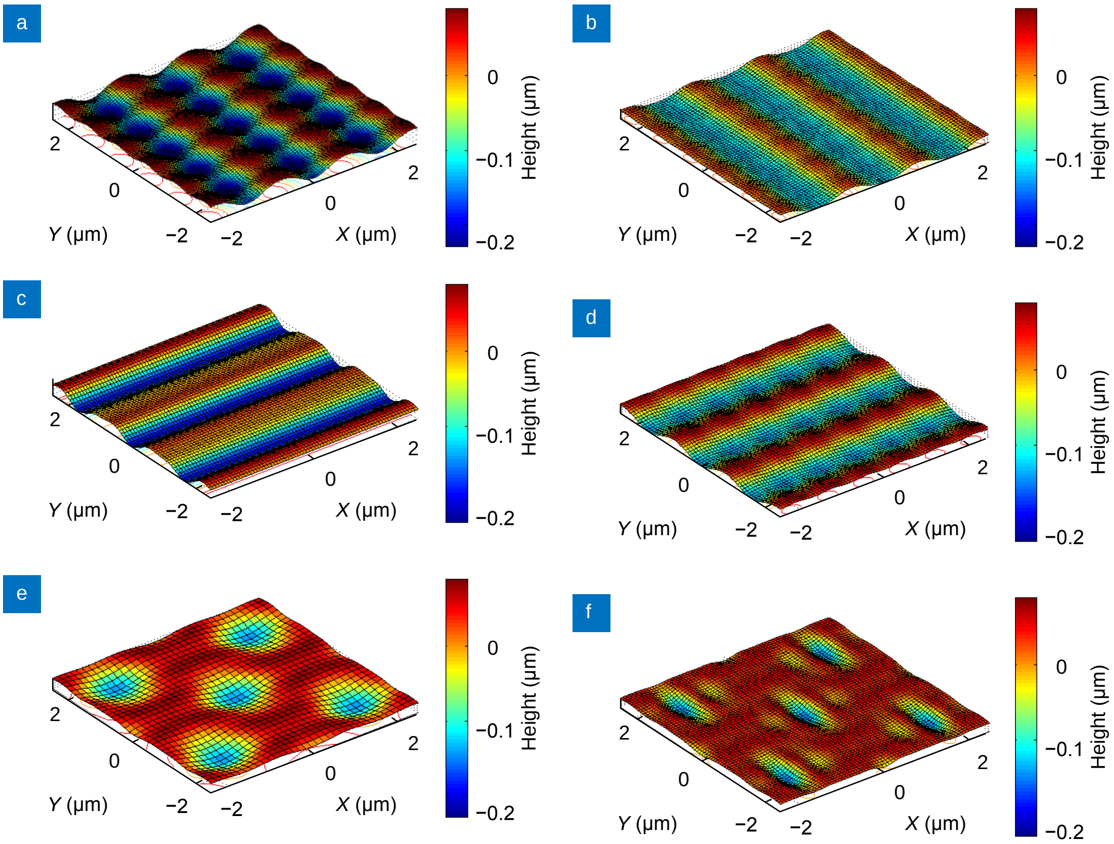

Fig. S10 | Spatial distribution of height for *NP* = 50 for (**a**) *G* + *V*, (**b**) *V* + *G*, (**c**) *G* + *H*, (**d**) *H* + *G*, (**e**) *G* + *D*, (**f**) *G* + *D*

References

1. Tsibidis GD, Barberoglou M, Loukakos PA, Stratakis E, Fotakis C. Dynamics of ripple formation on silicon surfaces by ultrashort laser pulses in subablation conditions. *Phys Rev B* **86**, 115316 (2012).
2. Fraggelakis F, Tsibidis GD, Stratakis E. Tailoring submicrometer periodic surface structures via ultrashort pulsed direct laser interference patterning. *Phys Rev B* **103**, 054105 (2021).
3. Pozrikidis C. *Introduction to Theoretical and Computational Fluid Dynamics* (Oxford University Press, New York, 1997).